Available online at www.sciencedirect.com
SCIENCE DIRECT®
Journal of Magnetism and Magnetic Materials 278 (2004) 270–284
www.elsevier.com/locate/jmmm

On the magnetostatic interactions between nanoparticles of arbitrary shape

M. Beleggia[a], S. Tandon[b], Y. Zhu[a], M. De Graef[b,*]

[a] *Materials Science Department, Brookhaven National Laboratory, Upton, NY 11973, USA*
[b] *Department of Materials Science and Engineering, Carnegie Mellon University, 5000 Forbes Avenue, Pittsburgh, PA 15213-3890, USA*

Received 23 October 2003; received in revised form 23 October 2003

Abstract

The general expression for the magnetostatic energy of two magnetized nanoparticles with arbitrary shape and magnetization state is derived within the framework of a Fourier space approach. It is shown how the standard dipole–dipole interaction, valid for large interparticle distances, should be modified in order to take into account the shape anisotropy of each particle. Explicit computations are given for a simple system of two interacting cylinders. For magnetic nanowires, i.e., cylinders with a very large aspect ratio, a simple derivation shows that the interaction is of monopolar, rather than dipolar, nature.

PACS: 41.20.Gz; 75.30.Gw; 75.40.Mg; 75.75.+a

Keywords: Shape amplitude; Magnetostatic energy; Dipolar interaction; Magnetic nanowires; Monopolar interaction

1. Introduction

Single-domain magnetic nanoparticles are possible candidates for information bits in high-density magnetic recording media [1,2]. To understand and control the miniaturization processes which will lead to ultra-high-density storage systems, it is necessary to properly analyze the interactions between the nanoparticles within the array, in particular, the effect of shape anisotropy in the case of non-spherical particles. To the best of our knowledge, the long-range magnetostatic interaction is often treated as if each nanoparticle were a pure dipole, which, as will be demonstrated, may result in large discrepancies for densely packed arrays. In some cases, a superficial treatment of magnetostatic coupling based on an unjustified extension of the demagnetizing factor concept leads to a large overestimate of the interaction effects [3]. It will be shown in this article how to properly take into account the effect of shape anisotropy on the magnetostatic coupling between magnetic particles of arbitrary shape and magnetization state.

It is often said in magnetism textbooks that analytical calculations regarding demagnetizing field and energy can be performed only if the magnet shapes are either ellipsoidal or prismatic [4]. It was recently shown [5–7] that this limitation is only apparent, and analytical calculations can be

*Corresponding author. Tel.: +1-412-268-8527; fax: +1-412-268-7596.
E-mail address: degraef@cmu.edu (M. De Graef).

0304-8853/$ - see front matter © 2003 Elsevier B.V. All rights reserved.
doi:10.1016/j.jmmm.2003.12.1314

performed in Fourier space for a huge class of particles, such as the faceted magnets and magnets with high-symmetry. For solids with some degree of symmetry, in particular for cylinders and shapes with rotational symmetry, the results can be expressed analytically in real space. In all other cases, a numerical inverse Fourier transform is required to compute the quantities of interest.

In this paper, we derive a new expression for the magnetostatic (dipolar) interaction energy between nanoparticles of arbitrary shape and magnetization state which takes into account the particle shape anisotropy without resorting to any approximation. Then, we specialize the formalism to particles with rotational symmetry, showing explicit results for interacting cylinders of variable aspect ratios (disks and rods) and special magnetization states (in-plane and axial).

The analysis presented in this article is purely magnetostatic. Other energy contributions, such as exchange, magneto-crystalline anisotropy, Zeeman, magnetoelastic, etc. are not considered. However, magnetostatic coupling is the most challenging interaction to be computed properly when shape anisotropy is involved, while other contributions can be treated in the standard real-space formalism which is, basically, the micromagnetic simulation framework.

The energy computation scheme presented in this article may contribute significantly to a proper understanding of magnetostatic coupling between nanoparticles or in general magnetic structures in the nanoscale, something which still lacks a complete and satisfactory overall picture, despite extensive numerical evaluations by micromagnetic simulations (often very time-consuming and problematic in defining shapes), mean field approximations [8] or phenomenological treatments [9].

First, we recall the foundation of the Fourier space framework for magnetostatic calculations, extending the results recently obtained [5–7] to interacting magnetized nanoparticles. Then, to verify the correctness of the procedure, we derive the standard dipole–dipole interaction, which is valid if the particles are spherical (the demagnetizing field outside a sphere is purely dipolar) or, as an approximation, when two shapes are interacting at large distances. In the following section, we present a general expression for the computation of the magnetostatic interaction energy when some degree of symmetry is present in the magnetic structures, in particular cylindrical symmetry. Finally, we specialize the analysis to interacting cylinders, in the form of disks and rods (nanowires).

2. Theoretical model

Let us first recall and extend the main results obtained in Ref. [5] to the treatment of shape anisotropy in a magnetic particle of arbitrary shape *and* magnetization state. Consider a magnetized particle with shape function $D(\mathbf{r})$ (equal to 1 inside and 0 outside the particle) and magnetization $M_0\hat{\mathbf{m}}(\mathbf{r})$. The magnetization vector field $\mathbf{M}(\mathbf{r})$ is then given by

$$\mathbf{M}(\mathbf{r}) = M_0 D(\mathbf{r})\hat{\mathbf{m}}(\mathbf{r}), \tag{1}$$

where the unit direction vector $\hat{\mathbf{m}}(\mathbf{r})$ has a different orientation in different points of a Cartesian reference system. In Fourier space, this relation can be written as $\mathbf{M}(\mathbf{k}) = M_0\mathbf{D}(\mathbf{k})$, with

$$\mathbf{D}(\mathbf{k}) \equiv \int D(\mathbf{r})\hat{\mathbf{m}}(\mathbf{r})\mathrm{e}^{-\mathrm{i}\mathbf{k}\cdot\mathbf{r}}\,\mathrm{d}\mathbf{r}. \tag{2}$$

As shown in Ref. [10], the magnetic vector potential in Fourier space is given by

$$\mathbf{A}(\mathbf{k}) = -\mathrm{i}\frac{\mu_0}{|\mathbf{k}|^2}[\mathbf{M}(\mathbf{k})\times\mathbf{k}] = -\mathrm{i}\frac{B_0}{|\mathbf{k}|^2}\mathbf{D}(\mathbf{k})\times\mathbf{k} \tag{3}$$

with $B_0 = \mu_0 M_0$. The magnetic induction $\mathbf{B}(\mathbf{r})$ is given by the curl of the vector potential $\mathbf{B} = \nabla\times\mathbf{A}$, which in Fourier space is equivalent to $\mathbf{B}(\mathbf{k}) = \mathrm{i}\mathbf{k}\times\mathbf{A}(\mathbf{k})$. Inserting Eq. (3) results in

$$\begin{aligned}\mathbf{B}(\mathbf{k}) &= \frac{B_0}{|\mathbf{k}|^2}\mathbf{k}\times[\mathbf{D}(\mathbf{k})\times\mathbf{k}]\\ &= B_0\left\{\mathbf{D}(\mathbf{k}) - \frac{\mathbf{k}[\mathbf{D}(\mathbf{k})\cdot\mathbf{k}]}{|\mathbf{k}|^2}\right\}.\end{aligned} \tag{4}$$

After an inverse Fourier transform, we obtain for the magnetic field around a non-uniformly magnetized particle with arbitrary shape

$$\mathbf{H}(\mathbf{r}) = -\frac{1}{8\pi^3}\int \mathrm{d}^3\mathbf{k}\,\frac{\mathbf{k}[\mathbf{M}(\mathbf{k})\cdot\mathbf{k}]}{|\mathbf{k}|^2}\mathrm{e}^{\mathrm{i}\mathbf{k}\cdot\mathbf{r}} \tag{5}$$

and also for the magnetic induction

$$\mathbf{B}(\mathbf{r}) = \mu_0[\mathbf{M}(\mathbf{r}) + \mathbf{H}(\mathbf{r})]. \tag{6}$$

The magnetostatic energy is generally defined as

$$E_\mathrm{m} = -\frac{\mu_0}{2}\int_V \mathbf{H}(\mathbf{r})\cdot\mathbf{M}(\mathbf{r})\,\mathrm{d}^3\mathbf{r}, \tag{7}$$

where the integral is taken over the volume of the particle. Inserting Eq. (5) and interchanging the order of the integrations, we arrive at

$$E_\mathrm{m} = \frac{\mu_0}{16\pi^3}\int \mathrm{d}^3\mathbf{k}\,\frac{|\mathbf{M}(\mathbf{k})\cdot\mathbf{k}|^2}{|\mathbf{k}|^2}. \tag{8}$$

This is the general expression for the magnetostatic energy of a non-uniformly magnetized particle with an arbitrary shape. In the case of uniform magnetization, we have $\mathbf{M}(\mathbf{k}) = M_0 D(\mathbf{k})\hat{\mathbf{m}}$, so that the energy becomes

$$E_\mathrm{m} = \frac{\mu_0 M_0^2}{16\pi^3}\int \mathrm{d}^3\mathbf{k}\,\frac{(\hat{\mathbf{m}}\cdot\mathbf{k})^2}{|\mathbf{k}|^2}|D(\mathbf{k})|^2, \tag{9}$$

an expression first reported by Beleggia and De Graef [5].

It is now straightforward to use Eq. (8) to derive the energy of interaction between two particles. Consider two particles with shape functions $D_i(\mathbf{r})$ and magnetization states $\mathbf{m}_i(\mathbf{r})$ $(i = 1, 2)$, located at positions $\mathbf{r}_i$. The origin of each particle is typically taken to be at the center of inversion, if one is present, otherwise any other point may be used. The total magnetization field is then given by

$$\begin{aligned}\mathbf{M}(\mathbf{r}) &= \mathbf{M}_1(\mathbf{r}-\mathbf{r}_1) + \mathbf{M}_2(\mathbf{r}-\mathbf{r}_2)\\ &= \sum_{i=1}^{2} M_i D_i(\mathbf{r}-\mathbf{r}_i)\hat{\mathbf{m}}(\mathbf{r}-\mathbf{r}_i).\end{aligned} \tag{10}$$

In Fourier space, the magnetization is represented by

$$\mathbf{M}(\mathbf{k}) = \sum_{i=1}^{2} M_i \mathbf{D}_i(\mathbf{k})\mathrm{e}^{\mathrm{i}\mathbf{k}\cdot\mathbf{r}_i}, \tag{11}$$

since a translation in direct space is equivalent to a phase shift in Fourier space. Substituting $\mathbf{M}(\mathbf{k})$ into Eq. (8), we obtain

$$\begin{aligned}E_\mathrm{m}(\mathbf{r}) = \frac{\mu_0}{16\pi^3}\int \frac{\mathrm{d}^3\mathbf{k}}{|\mathbf{k}|^2}\Bigg\{&\sum_{i=1}^{2}|\mathbf{M}_i(\mathbf{k})\cdot\mathbf{k}|^2\\ &+[\mathbf{M}_1(\mathbf{k})\cdot\mathbf{k}][\mathbf{M}_2^*(\mathbf{k})\cdot\mathbf{k}]\mathrm{e}^{\mathrm{i}\mathbf{k}\cdot\boldsymbol{\rho}}\\ &+[\mathbf{M}_1^*(\mathbf{k})\cdot\mathbf{k}][\mathbf{M}_2(\mathbf{k})\cdot\mathbf{k}]\mathrm{e}^{-\mathrm{i}\mathbf{k}\cdot\boldsymbol{\rho}}\Bigg\}\end{aligned} \tag{12}$$

with $\boldsymbol{\rho} = \mathbf{r}_1 - \mathbf{r}_2$, the vector connecting the two particles. This expression is equivalent to the following real space expression:

$$\begin{aligned}E_\mathrm{m} = -\frac{\mu_0}{2}\Bigg[&\sum_{i=1}^{2}\int_{V_i}\mathbf{H}_i(\mathbf{r})\cdot\mathbf{M}_i(\mathbf{r})\,\mathrm{d}^3\mathbf{r}\\ &+\int_{V_1}\mathbf{H}_2(\mathbf{r})\cdot\mathbf{M}_1(\mathbf{r})\,\mathrm{d}^3\mathbf{r}\\ &+\int_{V_2}\mathbf{H}_1(\mathbf{r})\cdot\mathbf{M}_2(\mathbf{r})\,\mathrm{d}^3\mathbf{r}\Bigg].\end{aligned} \tag{13}$$

Defining the self-energy as

$$E_i^\mathrm{self} \equiv \frac{\mu_0}{16\pi^3}\int \mathrm{d}^3\mathbf{k}\,\frac{|\mathbf{M}_i(\mathbf{k})\cdot\mathbf{k}|^2}{|\mathbf{k}|^2} \tag{14}$$

and combining the last two terms in Eq. (12), we obtain for the total magnetostatic energy

$$\begin{aligned}E_\mathrm{m}(\boldsymbol{\rho}) = \sum_{i=1}^{2} E_i^\mathrm{self} + \mu_0\,\Re\\ \times\left[\mathscr{F}^{-1}\left\{\frac{[\mathbf{M}_1(\mathbf{k})\cdot\mathbf{k}][\mathbf{M}_2^*(\mathbf{k})\cdot\mathbf{k}]}{|\mathbf{k}|^2}\right\}\right],\end{aligned} \tag{15}$$

where $\Re$ denotes the real part and $\mathscr{F}$ is the Fourier transform operator. The complex conjugate symbol can be placed on either one of the two factors $\mathbf{M}_i(\mathbf{k})$. The second term in this expression is the magnetostatic interaction energy between two particles with different shapes and magnetization states as a function of their relative position $\boldsymbol{\rho}$.

For particles with a uniform magnetization state, Eqs. (14) and (15) are replaced by

$$E_i^\mathrm{self} \equiv \frac{\mu_0 M_i^2}{16\pi^3}\int \mathrm{d}^3\mathbf{k}\,\frac{(\hat{\mathbf{m}}_i\cdot\mathbf{k})^2}{|\mathbf{k}|^2}|D_i(\mathbf{k})|^2 \tag{16}$$

and

$$E_{\mathrm{m}}(\boldsymbol{\rho}) = \sum_{i=1}^{2} E_i^{\mathrm{self}} + \mu_0 M_1 M_2 \Re \times \left[\mathscr{F}^{-1} \left\{ \frac{(\hat{\mathbf{m}}_1 \cdot \mathbf{k})(\hat{\mathbf{m}}_2 \cdot \mathbf{k})}{|\mathbf{k}|^2} D_1(\mathbf{k}) D_2^*(\mathbf{k}) \right\} \right]. \tag{17}$$

For particles with identical shape functions we also have $D_1(\mathbf{k})D_2^*(\mathbf{k}) = |D(\mathbf{k})|^2$.

In the following sections, we will present several applications of Eqs. (16) and (17). First, in Section 3, we derive the standard expression for the dipole–dipole interaction energy, starting from the shape amplitudes for two uniformly magnetized spheres. Then, in Section 4, we analyze the interaction energy between particles of identical shape, assuming that the particles possess some symmetry (in particular cylindrical). In Section 5, we specialize the results of Section 4 to the interaction between two uniformly magnetized cylinders. We present analytical expressions for the interaction energy for four different configurations of two cylinders: two adjacent cylinders with axial and in-plane magnetization states, and a stack of vertically displaced cylinders, again with axial and in-plane magnetization states. The energy expressions reduce to the standard dipole–dipole interactions for large particle separations, but describe significant corrections to the dipole approximation when the particles are close together. Finally, in Section 6, we analyze the case of semi-infinite cylinders, and we show that the dipolar interaction is no longer a valid description; instead, a monopolar, Coulomb-like interaction must be used.

3. Dipole–dipole interaction

To verify the correctness of the equations derived in the previous section, we will derive a well-known result, such as the expression for the dipole–dipole interaction. In order to obtain this result, we will consider two uniformly magnetized spheres of equal radius R, described by a shape amplitude [10]

$$D(\mathbf{k}) = \frac{4\pi R^2}{k} j_1(kR), \tag{18}$$

where $k = |\mathbf{k}|$, and $j_1(x)$ is the first-order spherical Bessel function. The spheres are separated from each other by the vector $\boldsymbol{\rho}$ (where we assume that $|\boldsymbol{\rho}| = \rho > 2R$, i.e., the spheres are not in contact or overlapping). Writing the double scalar product in Eq. (17) in terms of a sum over its components

$$(\hat{\mathbf{m}}_1 \cdot \mathbf{k})(\hat{\mathbf{m}}_2 \cdot \mathbf{k}) = \sum_{i,j=1}^{3} m_1^i m_2^j k_i k_j \tag{19}$$

and inserting the shape amplitude, we can write the interaction energy as

$$E^{\mathrm{int}}(\boldsymbol{\rho}; \hat{\mathbf{m}}_1, \hat{\mathbf{m}}_2) = \frac{2\mu_0 M_1 M_2 R^4}{\pi} \sum_{i,j=1}^{3} m_1^i m_2^j \int \mathrm{d}k j_1^2(kR) \times \int \mathrm{d}\Omega \frac{k_i k_j}{k^2} \mathrm{e}^{\mathrm{i}\mathbf{k}\cdot\boldsymbol{\rho}}. \tag{20}$$

Only the real part of the integral will be considered at the end, but, from a computational standpoint, the full complex exponential is more convenient.

The $k_i k_j / k^2$ term is purely angular when written in spherical coordinates, and was analyzed in Ref. [5] in connection with the derivation of the demagnetizing tensor of a sphere. The result of the angular integration over $\mathrm{d}\Omega$ is a combination of $j_0(k\rho)$ and $j_2(k\rho)$ spherical Bessel functions. After the final integration over k, we obtain the standard dipolar tensor to be summed over the magnetization components

$$E^{\mathrm{int}}(\boldsymbol{\rho}; \hat{\mathbf{m}}_1, \hat{\mathbf{m}}_2) = \frac{16\pi^2 \mu_0 M_1 M_2 R^4}{9} \sum_{i,j=1}^{3} m_1^i m_2^j \mathscr{D}_{ij}(\boldsymbol{\rho}) \tag{21}$$

with

$$\mathscr{D}(\boldsymbol{\rho}) = \frac{1}{4\pi\rho^5} \begin{pmatrix} \rho^2 - 3x^2 & -3xy & -3xz \\ -3xy & \rho^2 - 3y^2 & -3yz \\ -3xz & -3yz & \rho^2 - 3z^2 \end{pmatrix}, \tag{22}$$

the dipolar tensor. Now, defining the magnetic moment of each sphere as the product of magnetization and volume, i.e. $\boldsymbol{\mu}_i = 4/3\pi R^3 M_i \hat{\mathbf{m}}_i$, and performing the sum of the components as in

Eq. (19), we finally arrive at the standard dipole–dipole energy

$$E^{\mathrm{int}}(\boldsymbol{\rho};\boldsymbol{\mu}_1,\boldsymbol{\mu}_2)=\frac{\mu_0}{4\pi}\left[\frac{\boldsymbol{\mu}_1\cdot\boldsymbol{\mu}_2}{\rho^3}-3\,\frac{(\boldsymbol{\mu}_1\cdot\boldsymbol{\rho})(\boldsymbol{\mu}_2\cdot\boldsymbol{\rho})}{\rho^5}\right], \quad (23)$$

which is, of course, also valid in the limit for $R\to 0$, provided that each magnetic moment $\mu_i = M_i V$, with V the particle volume, remains finite.

In Ref. [5], we have introduced a Fourier space expression for the demagnetization tensor field $N_{ij}(\mathbf{k})$:

$$N_{ij}(\mathbf{k}) = D(\mathbf{k})\frac{k_i k_j}{k^2}. \quad (24)$$

If we convert this to real space we find an expression for the DTF, which was used in Ref. [6,7] to compute the DTF for the finite cylinder, and for a series of other important shapes. An interesting result can be obtained if we compute the inverse Fourier transform of Eq. (24), using the convolution theorem

$$N_{ij}(\mathbf{r}) = D(\mathbf{r})\otimes\mathscr{F}^{-1}\left[\frac{k_i k_j}{k^2}\right], \quad (25)$$

where $\otimes$ indicates the convolution product. The second function in this convolution product can be computed explicitly using cylindrical coordinates

$$\mathscr{F}^{-1}\left[\frac{k_i k_j}{k^2}\right] = \frac{1}{8\pi^3}\int_0^{2\pi}\mathrm{d}\theta\int_{-\infty}^{+\infty}\mathrm{d}k_z\mathrm{e}^{\mathrm{i}k_z z} \times\int_0^{\infty}\mathrm{d}k k\,\frac{k_i k_j}{k^2+k_z^2}\mathrm{e}^{\mathrm{i}kr\cos(\theta-\theta')}. \quad (26)$$

A straightforward integration followed by a conversion to Cartesian coordinates reveals that this integral is equal to the tensor field $\mathscr{D}_{ij}$ introduced earlier:

$$N_{ij}(\mathbf{r}) = D(\mathbf{r})\otimes\mathscr{D}_{ij}(\mathbf{r}). \quad (27)$$

If we consider a point dipole, with shape function $\delta(\mathbf{r})$, then we find

$$N_{ij}(\mathbf{r}) = \delta(\mathbf{r})\otimes\mathscr{D}_{ij}(\mathbf{r}) = \mathscr{D}_{ij}(\mathbf{r}), \quad (28)$$

where we have used the fact that the delta-function is the identity function for the convolution product. In other words, the DTF for a single dipole is the tensor field $\mathscr{D}_{ij}(\mathbf{r})$. The DTF for an object of arbitrary shape is the convolution of the dipole DTF with the shape function of the object. In other words, the dipole tensor field is copied at every point of the object to obtain the full DTF.

4. Interactions between magnetic particles of identical shape

Consider two point dipoles with magnetic moments $\boldsymbol{\mu}_i$, located at a relative position $\boldsymbol{\rho}$. The interaction energy between these dipoles is given by

$$E^{\mathrm{int}}(\boldsymbol{\rho}) = \frac{\mu_0}{4\pi}\left[\frac{\boldsymbol{\mu}_1\cdot\boldsymbol{\mu}_2}{\rho^3}-3\,\frac{(\boldsymbol{\mu}_1\cdot\boldsymbol{\rho})(\boldsymbol{\mu}_2\cdot\boldsymbol{\rho})}{\rho^5}\right]. \quad (29)$$

Working in cylindrical coordinates, we can write the moments as $\boldsymbol{\mu}_i = (\mu_i^{\perp}\cos\theta_i, \mu_i^{\perp}\sin\theta_i, \mu_i^z)$ with $\mu_i^2 = (\mu_i^{\perp})^2 + (\mu_i^z)^2$, and the position vector as $\boldsymbol{\rho} = (r\cos\theta_r, r\sin\theta_r, z)$, with $\rho^2 = r^2 + z^2$. The interaction energy is then given in component notation by

$$\begin{aligned}E^{\mathrm{int}}(\boldsymbol{\rho}) = \frac{\mu_0}{4\pi}\Bigg[&\frac{\mu_1^{\perp}\mu_2^{\perp}}{\rho^3}\cos(\theta_1-\theta_2)+\frac{(r^2-2z^2)}{\rho^5}\mu_1^z\mu_2^z\\ &-\frac{3}{\rho^5}\big\{r^2\mu_1^{\perp}\mu_2^{\perp}\cos(\theta_1-\theta_r)\cos(\theta_2-\theta_r)\\ &+rz[\mu_1^{\perp}\mu_2^z\cos(\theta_1-\theta_r)\\ &+\mu_2^{\perp}\mu_1^z\cos(\theta_2-\theta_r)]\big\}\Bigg]. \end{aligned} \quad (30)$$

We will next determine how this expression changes when the dipoles are replaced by two identical objects with uniform magnetization and cylindrical symmetry. Consider the shape amplitude for an object with cylindrical symmetry, as defined in Ref. [6]. The shape amplitude can be written as

$$D(\mathbf{k}) = \frac{2\pi}{k}\int_{h_1}^{h_2}\mathrm{d}z' f(k,z')\mathrm{e}^{-\mathrm{i}z'k_z}, \quad (31)$$

where $\mathbf{k} = (k\cos\theta, k\sin\theta, k_z)$ and $k^2 + k_z^2 = K^2$. The function $f(k,z')$ is defined as

$$f(k,z') \equiv r_2(z')J_1(kr_2(z')) - r_1(z')J_1(kr_1(z')), \quad (32)$$

where $J_1(x)$ is the Bessel function of the first kind, and the functions $r_i(z')$ describe the inner and outer surfaces of the object, as shown in Fig. 1. The interaction energy between two such objects located at relative position $\boldsymbol{\rho}$ and with identical

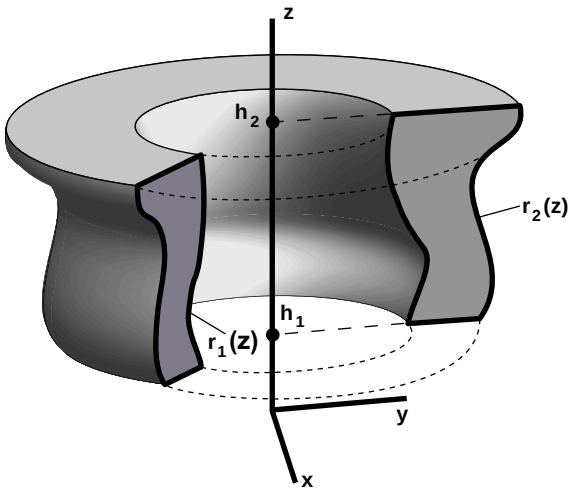

Fig. 1. Schematic representation of a general object of revolution with distinct inner and outer surfaces $r_1(z)$ and $r_2(z)$.

orientation, is given by

$$E^{\mathrm{int}}(\boldsymbol{\rho}) = \mu_0 M_1 M_2 \Re \times \left[\mathscr{F}^{-1} \left\{ \frac{(\hat{\mathbf{m}}_1 \cdot \mathbf{k})(\hat{\mathbf{m}}_2 \cdot \mathbf{k})}{K^2} |D(\mathbf{k})|^2 \right\} \right], \quad (33)$$

which becomes

$$E^{\mathrm{int}}(\boldsymbol{\rho}) = \frac{\mu_0 M_1 M_2}{2\pi} \Re \times \left[\int \frac{\mathrm{d}^3\mathbf{k}}{K^2} \frac{(\hat{\mathbf{m}}_1 \cdot \mathbf{k})(\hat{\mathbf{m}}_2 \cdot \mathbf{k})}{k^2} \times \left| \int_{h_1}^{h_2} \mathrm{d}z' f(k, z') \mathrm{e}^{-\mathrm{i}z'k_z} \right|^2 \mathrm{e}^{\mathrm{i}\mathbf{k}\cdot\boldsymbol{\rho}} \right]. \quad (34)$$

Writing the modulus squared factor as $F(k, k_z)$, we arrive at

$$E^{\mathrm{int}}(\boldsymbol{\rho}) = \frac{\mu_0 M_1 M_2}{2\pi} \Re \left[\int_0^\infty \frac{\mathrm{d}k}{k} \int_{-\infty}^{+\infty} \mathrm{d}k_z \frac{F(k, k_z) \mathrm{e}^{\mathrm{i}zk_z}}{k^2 + k_z^2} \times \int_0^{2\pi} \mathrm{d}\theta (\hat{\mathbf{m}}_1 \cdot \mathbf{k})(\hat{\mathbf{m}}_2 \cdot \mathbf{k}) \mathrm{e}^{\mathrm{i}kr\cos(\theta - \theta_r)} \right]. \quad (35)$$

The angular integral can be solved by noting that

$$(\hat{\mathbf{m}}_1 \cdot \mathbf{k})(\hat{\mathbf{m}}_2 \cdot \mathbf{k}) = m_1^\perp m_2^\perp k^2 \cos(\theta_1 - \theta)\cos(\theta_2 - \theta) + m_1^z m_2^z k_z^2 + k k_z [m_1^\perp m_2^z \cos(\theta_1 - \theta) + m_2^\perp m_1^z \cos(\theta_2 - \theta)]. \quad (36)$$

The resulting integral is given by

$$2\pi m_1^\perp m_2^\perp \left[\frac{k}{r} J_1(kr) \cos(\theta_1 - \theta_2) - k^2 J_2(kr) \cos(\theta_1 - \theta_r) \cos(\theta_2 - \theta_r) \right] - 2\pi \mathrm{i} k k_z J_1(kr) \left[m_1^\perp m_2^z \cos(\theta_1 - \theta_r) + m_2^\perp m_1^z \cos(\theta_2 - \theta_r) \right] + 2\pi m_1^z m_2^z k_z^2 J_0(kr), \quad (37)$$

where the functions $J_i(x)$ are Bessel functions of the first kind. Note that the angular terms in this expression are identical to the terms in Eq. (30). Introducing the magnetic moments as $\boldsymbol{\mu}_i = V M_i \hat{\mathbf{m}}_i$, substituting Eq. (37) into Eq. (35), and rearranging terms we find

$$E^{\mathrm{int}}(\boldsymbol{\rho}) = \frac{\mu_0}{4\pi} \left[\frac{\mu_1^\perp \mu_2^\perp}{\rho^3} S_1(r, z; \mathbf{s}) \cos(\theta_1 - \theta_2) + \frac{(r^2 - 2z^2)}{\rho^5} \mu_1^z \mu_2^z S_2(r, z; \mathbf{s}) - \frac{3}{\rho^5} \{ r^2 \mu_1^\perp \mu_2^\perp S_3(r, z; \mathbf{s}) \times \cos(\theta_1 - \theta_r) \cos(\theta_2 - \theta_r) + rz S_4(r, z; \mathbf{s}) [\mu_1^\perp \mu_2^z \cos(\theta_1 - \theta_r) + \mu_2^\perp \mu_1^z \cos(\theta_2 - \theta_r)] \} \right], \quad (38)$$

where the functions $S_i(r, z; \mathbf{s})$ are defined by

$$S_1(r, z; \mathbf{s}) = \frac{8\pi\rho^3}{rV^2} \int_0^\infty \mathrm{d}k J_1(kr) \times \int_0^\infty \mathrm{d}k_z \frac{F(k, k_z) \cos(zk_z)}{k^2 + k_z^2}, \quad (39)$$

$$S_2(r, z; \mathbf{s}) = \frac{8\pi\rho^5}{(r^2 - 2z^2)V^2} \int_0^\infty \frac{\mathrm{d}k}{k} J_0(kr) \times \int_0^\infty \mathrm{d}k_z \frac{k_z^2 F(k, k_z) \cos(zk_z)}{k^2 + k_z^2}, \quad (40)$$

$$S_3(r, z; \mathbf{s}) = \frac{8\pi\rho^5}{3r^2V^2} \int_0^\infty \mathrm{d}k k J_2(kr) \times \int_0^\infty \mathrm{d}k_z \frac{F(k, k_z) \cos(zk_z)}{k^2 + k_z^2}, \quad (41)$$

$$S_4(r,z;\mathbf{s}) = -\frac{8\pi\rho^5}{3rzV^2}\int_0^\infty \mathrm{d}kJ_1(kr) \times \int_0^\infty \mathrm{d}k_z \frac{k_z F(k,k_z)\sin(zk_z)}{k^2+k_z^2} \quad (42)$$

and the vector $\mathbf{s}$ represents all the parameters that define the shape of the object. The angular dependence of the interaction energy (38) is identical to that of the pure dipole case in Eq. (30), but each of the four terms is weighted by a position- and shape-dependent correction factor $S_i(r,z;\mathbf{s})$.

Consider next two special configurations of the two particles: (1) both particles have their center in the plane $z=0$, and (2) both particles are aligned along the z-axis, so that $r=0$. The interaction energy for those two cases is given by the following expressions:

$$E_h^{\mathrm{int}}(r,0) = \frac{\mu_0}{4\pi r^3}[\mu_1^\perp\mu_2^\perp S_1(r,0;\mathbf{s})\cos(\theta_1-\theta_2) + \mu_1^z\mu_2^z S_2(r,0;\mathbf{s}) - 3\mu_1^\perp\mu_2^\perp S_3(r,0;\mathbf{s}) \times \cos(\theta_1-\theta_r)\cos(\theta_2-\theta_r)], \quad (43)$$

$$E_v^{\mathrm{int}}(0,z) = \frac{\mu_0}{4\pi z^3}[\mu_1^\perp\mu_2^\perp S_1(0,z;\mathbf{s})\cos(\theta_1-\theta_2) - 2\mu_1^z\mu_2^z S_2(0,z;\mathbf{s})]. \quad (44)$$

Note that the function $S_4(r,z;\mathbf{s})$ only enters the equation when both r and z are different from zero. For particles of finite size, all four integrals S_i must approach 1, when the particles are sufficiently far removed from each other, i.e., the interactions must approach the pure dipolar interactions. When the distance between the particles is small, comparable to their dimensions, significant deviations from the pure dipolar behavior may be expected. In the following section, we will analyze the special cases (43) and (44) for the interaction between two identical uniformly magnetized disks.

5. Interactions between identical magnetic disks

In this section, we will apply Eqs. (43) and (44) to the interaction between two uniformly magnetized disks with arbitrary aspect ratio. The energy of interaction between disks is usually considered as purely dipolar, if the disks are sufficiently far away from each other. A numerical analysis was performed in Ref. [11] in order to verify this approximation. However, this analysis was only numerical, as the expression of the interaction energy between disks is not yet known. The goal of this section is to show that we can derive an analytical expression for the magnetic energy of two disks, which consists of a modification of the standard dipole–dipole interaction. It will be shown that, in the limit where the disks are widely separated, the approximation of pure dipole–dipole interaction is justified. However, by means of our approach, we can provide further insight on the matter. In particular, it will be shown that for two disks sufficiently close to each other, there are significant deviations from the dipolar behavior. This may have a dramatic impact in the study of the energetics of arrays of nanoparticles.

We begin by computing the function $F(k,k_z)$ for a disk with radius R, height $2d$, and volume V. Since, for the cylinder, we have $f(k,z') = RJ_1(kR)$, we find

$$F(k,k_z) = 4R^2J_1^2(kR)\frac{\sin^2(dk_z)}{k_z^2}. \quad (45)$$

The cylinder aspect ratio is defined as $\tau \equiv d/R$. The self-energy can be computed using Eq. (16) and was reported in Ref. [6]. It can be expressed as a function of the aspect ratio τ and the component m_z of the unit magnetization vector $\hat{\mathbf{m}}$:

$$E_{\mathrm{m}}^{\mathrm{self}}(\tau,m_z) = \frac{\mu_0 M_0^2 R^3}{6}\left[4(3m_z^2-1) + 6\pi\tau m_z^2 - 3\pi\sqrt{1+\tau^2}(3m_z^2-1) \times {}_2F_1\left(-\frac{1}{2},\frac{3}{2};2;\frac{1}{1+\tau^2}\right)\right] \quad (46)$$

with ${}_2F_1(a,b;c;z)$ a hypergeometric series. For $\tau<\tau_c \equiv 0.90647$, the in-plane magnetization state with $m_z=0$ has the lowest energy, while for $\tau>\tau_c$, the axial magnetization state is preferred.

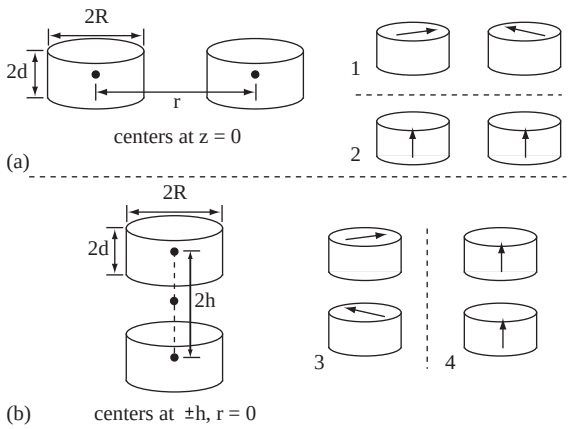

Fig. 2. Graphical representation of the two configurations considered in this paper. For each configuration, two different magnetization arrangements (in-plane (a) and axial (b)) are considered.

In the remainder of this section we will consider two special configurations of the two disks, as shown in Fig. 2. In configuration (a), both disks are located in the same plane $z = 0$ at a center-to-center distance r. In configuration (b), the disks are aligned along the z-axis ($r = 0$) at a center-to-center distance $2h$. It will be useful to define two dimensionless quantities ρ and ζ

$$\rho \equiv \frac{2R}{r}, \qquad \zeta \equiv \frac{h}{d}. \tag{47}$$

When the two disks touch in configuration (a), we have $\rho = 1$; at infinite separation $\rho = 0$. For configuration (b), the disks touch when $\zeta = 1$. For each configuration, we will analyze the interaction energy for both in-plane (1 and 3 in Fig. 2) and axial (2 and 4) magnetization states. The argument $\mathbf{s}$ of the functions $S_i(r, z; \mathbf{s})$ will be equal to $\mathbf{s} = (R, t)$, the dimensional parameters of the cylinder. In dimensionless units, the relevant integrals will be represented by $S_i(\rho, \tau)$ and $S_i(\zeta, \tau)$.

Next, we will derive analytical expressions for the interaction energy for all four cases of Fig. 2. Following the derivations, we will analyze the results and compare them to the standard dipole–dipole interaction.

5.1. Case 1

The interaction energy (43) in this case can be written as

$$E_h^{\mathrm{int}}(r,0) = \frac{\mu_0}{4\pi}\left[\frac{\boldsymbol{\mu}_1 \cdot \boldsymbol{\mu}_2}{r^3} S_1(r,0;R,t) - 3\frac{(\boldsymbol{\mu}_1 \cdot \mathbf{r})(\boldsymbol{\mu}_2 \cdot \mathbf{r})}{r^5} S_3(r,0;R,t)\right]. \tag{48}$$

Since both disks are located in the plane $z = 0$, the k_z integral for both S_1 and S_3 can be shown to be equal to

$$\int_0^\infty \frac{\mathrm{d}k_z}{k_z^2}\frac{\sin^2(dk_z)}{k^2 + k_z^2} = \frac{\pi}{k^3}[kt - 1 + \mathrm{e}^{-kt}]. \tag{49}$$

Expression (48) has the familiar dipole–dipole form, with the exception of the two functions $S_i(r, 0; R, t)$ which are defined by the following relations (dropping the $\perp$ on k):

$$S_1(r,0;R,t) \equiv \frac{8r^2}{R^2t^2}\int_0^{+\infty}\frac{\mathrm{d}k}{k^3}J_1^2(kR)J_1(kr)[kt - 1 + \mathrm{e}^{-kt}], \tag{50}$$

$$S_3(r,0;R,t) \equiv \frac{8r^3}{3R^2t^2}\int_0^{+\infty}\frac{\mathrm{d}k}{k^2}J_1^2(kR)J_2(kr)[kt - 1 + \mathrm{e}^{-kt}]. \tag{51}$$

Since there is no known analytical solution for these integrals, they must be solved numerically. It is possible, however, to simplify the integrals for a thin disk, i.e., when $t \ll R$. In that case, we can expand the exponential e^{-kt} to second order, and only the term in k^2t^2 remains. If we represent the approximate integrals as G_i, then we find

$$\frac{4r^2}{R^2}\int_0^{+\infty}\frac{\mathrm{d}k}{k}J_1^2(kR)J_1(kr) = {}_3F_2\left(\frac{1}{2},\frac{3}{2},\frac{3}{2};2,3;\rho^2\right) \equiv G_1(\rho), \tag{52}$$

$$\frac{4r^3}{3R^2}\int_0^{+\infty}\mathrm{d}kJ_1^2(kR)J_2(kr) = {}_3F_2\left(\frac{1}{2},\frac{3}{2},\frac{5}{2};2,3;\rho^2\right) \equiv G_2(\rho), \tag{53}$$

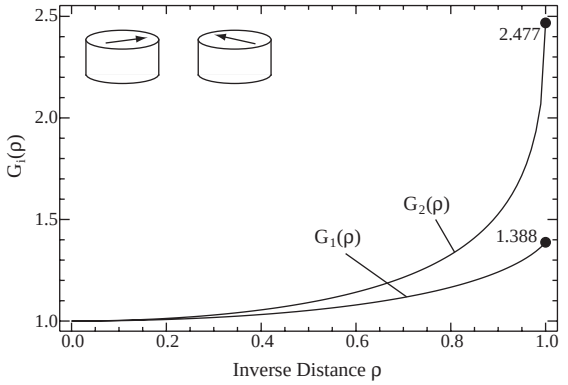

Fig. 3. Graphical representation of the functions $G_i(\rho)$, defined in Eqs. (52) and (53).

where ρ was defined in Eq. (47). The functions ${}_3F_2(\ldots)$ are generalized hypergeometric series. There is no longer a thickness dependence in the approximate integrals; the thickness t only appears in the definition of the magnetic moments $\boldsymbol{\mu}_i$. The functions G_1 and G_2, shown in Fig. 3, can be interpreted as an indication of the modified balance between the two driving forces in the dipole–dipole interaction. In fact, G_1 and G_2 can be seen as a coefficient assigned to the two terms in Eq. (48): the first represents a tendency to keep the moments antiparallel, while the tendency in the second term is to keep the moments aligned along the direction connecting them. In the pure dipole–dipole interaction, for instance when we have spherical particles, the relative coefficients for the two terms are $(1,-3)$, while in the shape-anisotropy corrected expression, valid for cylinders of small aspect ratio, the coefficient become $(G_1,-3G_2)$.

The self-energy of the uniformly magnetized cylinder was derived analytically by Tandon et al. [6], and is given (for in-plane magnetization) by

$$E_i^{\text{self}} = \frac{\mu_0 M_i^2 R^2}{12}\left[-8R + 3\pi t\, {}_2F_1\left(-\frac{1}{2},\frac{1}{2};2;-\frac{1}{\tau^2}\right)\right] \tag{54}$$

with ${}_2F_1[\ldots]$ a hypergeometric series. If we express the self-energy in terms of the magnetic moments, and expand the energy with respect to the disk aspect ratio τ, we find the following expression:

$$E_i^{\text{self}} = \frac{\mu_0}{4\pi}\frac{\boldsymbol{\mu}_i\cdot\boldsymbol{\mu}_i}{\pi R^3}\left(\ln\frac{4}{\tau}-\frac{1}{2}\right). \tag{55}$$

The total magnetostatic energy for a pair of identical thin interacting disks with in-plane magnetic moments $\boldsymbol{\mu}_1$ and $\boldsymbol{\mu}_2$ is then given by

$$\begin{aligned} &E_{\text{m}}(\mathbf{r};\boldsymbol{\mu}_1,\boldsymbol{\mu}_2)\\ &\quad=\frac{\mu_0}{4\pi}\left[\frac{|\boldsymbol{\mu}_1|^2+|\boldsymbol{\mu}_2|^2}{\pi R^3}\left(\ln\frac{4}{\tau}-\frac{1}{2}\right)\right.\\ &\qquad\left.+\frac{\boldsymbol{\mu}_1\cdot\boldsymbol{\mu}_2}{r^3}G_1(\rho)-3\frac{(\boldsymbol{\mu}_1\cdot\mathbf{r})(\boldsymbol{\mu}_2\cdot\mathbf{r})}{r^5}G_2(\rho)\right]. \end{aligned} \tag{56}$$

The total energy, including the self-energy, of a pair of parallel cylinders, not necessarily thin, with parallel in-plane magnetization can be written in dimensionless form as

$$\begin{aligned} &\bar{E}_h^{\text{tot}}(\rho,\tau)\\ &\quad=\frac{\sqrt{1+\tau^2}}{\tau^2}\,{}_2F_1\left(-\frac{1}{2},\frac{3}{2};2;\frac{1}{1+\tau^2}\right)\\ &\qquad-\frac{4}{3\pi\tau^2}+\frac{\rho^3}{8}[S_1(\rho,\tau)-3S_3(\rho,\tau)], \end{aligned} \tag{57}$$

where the overbar on the energy indicates a normalization by the factor $\mu_0|\mu_1||\mu_2|/4\pi R^3$.

5.2. Case 2

For the axial magnetization state, the interaction energy (43) becomes

$$E_h^{\text{int}}(r,0) = \frac{\mu_0}{4\pi}\frac{|\boldsymbol{\mu}_1|\,|\boldsymbol{\mu}_1|\alpha_1\alpha_2}{r^3}S_2(r,0;R,t), \tag{58}$$

where $\alpha_i=\pm 1$ for the two magnetization states. The k_z-integral in $S_2(r,0;R,t)$ for $z=0$ can be shown to be equal to

$$\int_0^\infty \mathrm{d}k_z\,\frac{\sin^2(dk_z)}{k^2+k_z^2}=\frac{\pi}{k}(1-\mathrm{e}^{-kt}),$$

which leads to

$$S_2(\rho,\tau)\equiv\frac{16}{\rho^3\tau^2}\int_0^\infty \mathrm{d}q\,\frac{J_1^2(q)}{q^2}J_0\left(\frac{2q}{\rho}\right)[1-\mathrm{e}^{-2q\tau}]. \tag{59}$$

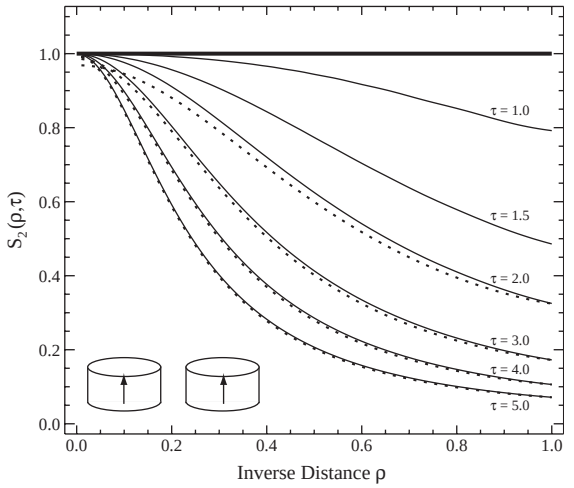

Fig. 4. Schematic of the function $S_2(\rho,\tau)$ for a number of aspect ratios τ. At $\rho = 0$, the cylinders have an infinite separation, whereas they are in contact for $\rho = 1$. The dotted lines represent the approximation of Eq. (61).

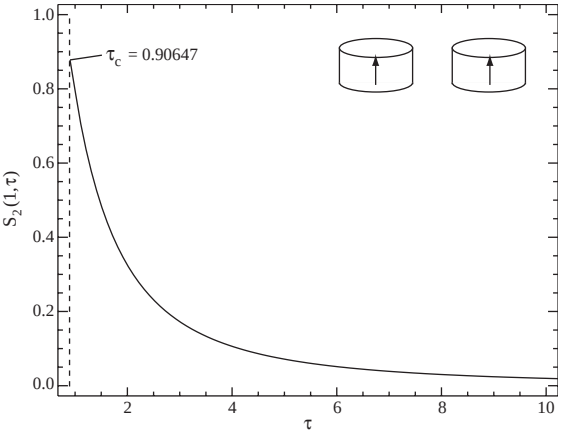

Fig. 5. Graphical representation of the function $S_2(\rho,\tau)$ for $\rho = 1$ (cylinders in contact). The smallest value of τ is equal to $\tau_c = 0.90647$, which is the point at which the vertical magnetization has the lowest self-energy for cylinders with infinite separation distance. The larger the aspect ratio, the larger the deviation from the dipolar approximation for which S_2 would be equal to 1 for all parameter values.

Expanding $J_1^2(q)/q^2$ in a Taylor series around $q = 0$ and integrating term by term we obtain

$$S_2(\rho,\tau) = \frac{2}{\rho^2\tau^2}\,{}_3F_2\left(\frac{1}{2},\frac{1}{2},\frac{2}{3};2,3;\rho^2\right) - \frac{4}{\rho^3\tau^3}\sum_{n=0}^{\infty}\frac{(-1)^n(2n)!(2n+1)!}{2^{4n}(n!)^2(n+1)!(n+2)!\tau^{2n}} \times {}_2F_1\left(n+\frac{1}{2},n+1;1;-\frac{1}{\rho^2\tau^2}\right), \quad (60)$$

where ${}_2F_1[\ldots]$ is the standard hypergeometric series. An approximate value can be obtained if we assume that the aspect ratio τ is large; retaining only the first two terms of the series expansion above we have

$$S_2(\rho,\tau) \approx \frac{1}{\tau^2}\left[\frac{2\rho^2\tau^2-1}{8(1+\rho^2\tau^2)^{5/2}} - \frac{2}{\rho^2\sqrt{1+\rho^2\tau^2}} + \frac{2}{\rho^2}\,{}_3F_2\left(\frac{1}{2},\frac{1}{2},\frac{2}{3};2,3;\rho^2\right)\right]. \quad (61)$$

This approximation results in an error of less than 3% for $\tau > 2$. In the limit $\rho \to 0$, i.e., a large separation between the rods, the function $S_2(\rho,\tau)$ approaches 1 for all aspect ratios τ, so that we recover the standard dipole–dipole interaction energy in equation (58). The function $S_2(\rho,\tau)$ is shown in Fig. 4 for a range of aspect ratios τ. The solid horizontal line corresponds to the standard dipole–dipole approximation. The dotted lines were computed using the approximate equation (61); for large values of τ, the approximation is rather good. Fig. 5 shows the function $S_2(1,\tau)$ for a continuous range of aspect ratios.

The normalized total energy, including the self-energy, of a pair of parallel cylinders with anti-parallel axial magnetization can be written as

$$\tilde{E}_v^{\mathrm{tot}}(\rho,\tau) = \frac{8}{3\pi\tau^2} + \frac{2}{\tau} - \frac{2\sqrt{1+\tau^2}}{\tau^2} \times {}_2F_1\left(-\frac{1}{2},\frac{3}{2};2;\frac{1}{1+\tau^2}\right) - \frac{\rho^3}{8}S_2(\rho,\tau). \quad (62)$$

5.3. Case 3

For two disks positioned on top of one another, with in-plane magnetization vectors, we can proceed along similar lines as in the preceding

cases. The interaction energy (44) for in-plane magnetization can be written as

$$E_v^{\mathrm{int}}(0,z) = \frac{\mu_0}{4\pi}\frac{\boldsymbol{\mu}_1\cdot\boldsymbol{\mu}_2}{z^3}S_1(0,z;R,t) \tag{63}$$

with, in dimensionless form

$$\begin{aligned} S_1(\zeta,\tau) &\equiv 32\zeta^3\tau\int_0^\infty \mathrm{d}q\,\frac{J_1^2(q)}{q^2}\mathrm{e}^{-q2\zeta\tau}(\cosh(2q\tau)-1),\\ &= 8\zeta^3\tau\sum_{n=-1}^{+1} c_n[4+(2\zeta+n)^2\tau^2]^{1/2}\\ &\quad\times {}_2F_1\left(-\frac{1}{2},\frac{1}{2};2;\frac{4}{4+(2\zeta+n)^2\tau^2}\right) \end{aligned} \tag{64}$$

and $c_{-1,0,1} = [1,-2,1]$. It is easily verified that $S_1(\infty,\tau) = 1$, so that the dipolar approximation is again a good one for a large separation distance.

The normalized total energy, including the self-energy, of a pair of parallel cylinders aligned along the z-direction with in-plane magnetization can be written as

$$\begin{aligned} \bar{E}_h^{\mathrm{tot}}(\zeta,\tau) &= \frac{\sqrt{1+\tau^2}}{\tau^2}\,{}_2F_1\left(-\frac{1}{2},\frac{3}{2};2;\frac{1}{1+\tau^2}\right)\\ &\quad -\frac{4}{3\pi\tau^2}+\frac{1}{8\tau^3\zeta^3}S_1(\zeta,\tau). \end{aligned} \tag{65}$$

5.4. Case 4

Finally, for a stack of two disks with axial magnetization, we find that the interaction energy (44) is described by

$$E_v^{\mathrm{int}}(0,z) = -\frac{\mu_0}{4\pi}\frac{\boldsymbol{\mu}_1\cdot\boldsymbol{\mu}_2}{z^3}2S_2(0,z;R,t). \tag{66}$$

As shown in the appendix, the functions $S_1(r,z;R,t)$ and $S_2(r,z;R,t)$ are identical in the limit $r\to 0$, so that the normalized total energy for this case is given by

$$\begin{aligned} &\bar{E}_v^{\mathrm{tot}}(\zeta,\tau)\\ &\quad= \frac{8}{3\pi\tau^2}+\frac{2}{\tau}-\frac{2\sqrt{1+\tau^2}}{\tau^2}\\ &\qquad\times {}_2F_1\left(-\frac{1}{2},\frac{3}{2};2;\frac{1}{1+\tau^2}\right)-\frac{1}{4\tau^3\zeta^3}S_1(\zeta,\tau). \end{aligned} \tag{67}$$

5.5. Discussion

The result for case 1 is strikingly similar to the dipole–dipole energy found in Eq. (23), the only difference being the two hypergeometric functions, which do not depend on the magnetization angles, but only on the ratio of the diameter to the distance between the disks. Fig. 3 indicates that, in the limit for $r \gg 2R$ (i.e., $\rho\to 0$), both hypergeometric functions tend to 1, thus confirming that sufficiently far away the disks can be treated as pure dipoles. However, when the disks are close enough to each other, there are strong deviations from the dipole–dipole interaction. The maximum difference is reached when the disks are in contact, or $\rho = 1$. In this case, the two hypergeometric functions reach their maximum value, which is 1.388 for $G_1(1)$ and 2.477 for $G_2(1)$. It is evident that the deviation from the dipolar interaction is rather dramatic, reaching in some particular configurations even a factor of three, such as for two disks with magnetization $(1,0)$ and a separation vector $(2R,0)$ (Cartesian), where the dipolar energy gives -0.25 while the correct expression, using the approximate integrals $G_i(\rho)$, results in -0.755.

Fig. 6 shows a comparison between the magnetostatic interaction energy in the dipole approximation (a) (i.e., $G_i = 1$) and the energy for the interacting disks (b) as a function of the dipole angles θ_1 and θ_2 (these are the angles between the dipole moments and the line connecting the centers of the disks). Both grayscale plots use the same absolute scale; it is clear that the energy minima for the disks are significantly deeper than for the dipole approximation. This is also shown in the linear plot in Fig. 6(c), which represents both energies as a function of θ_1 for $\theta_2 = 0$.

To better evaluate when the dipolar approximation is appropriate, we can simply check the value of the two hypergeometric functions for a certain value of the ratio ρ. For instance, when the distance between the disks is equal to 10 times their radius ($\rho = \frac{1}{5}$), we have $G_1(\frac{1}{5}) = 1.008$ and $G_2(\frac{1}{5}) = 1.012$. In this condition, we can approximate the energy as dipolar within, roughly, 1% accuracy.

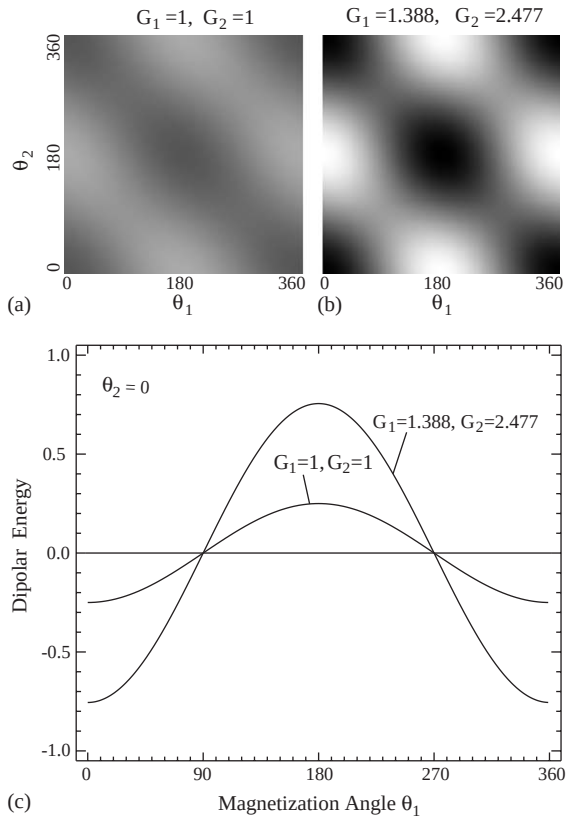

Fig. 6. Graphical representation of the magnetostatic interaction energy for two dipoles (a) and two magnetized disks in contact (b) as a function of the magnetization direction angles θ_i; the graylevels are represented on a common scale. In (c), the energy curves for $\theta_2 = 0$ are compared; the interacting disks have a significantly deeper energy minimum for $\theta_1 = 0$ than the pure dipoles.

We can combine the normalized total energies for cases 1 and 2 or 3 and 4 to determine how the critical aspect ratio τ_c for a single cylinder is affected by the presence of the second cylinder. Fig. 7 shows a contour plot of $\bar{E}_v^{\mathrm{tot}}(\rho,\tau) - \bar{E}_h^{\mathrm{tot}}(\rho,\tau)$, using Eqs. (57) and (62); the thicker contour indicates the critical aspect ratio $\tau_c(\rho)$ as a function of the separation distance between the two cylinders. When the cylinders touch each other, the critical aspect ratio $\tau_c(1) = 1.0921$. The presence of the second cylinder stabilizes the in-plane magnetization orientation with respect to the axial orientation.

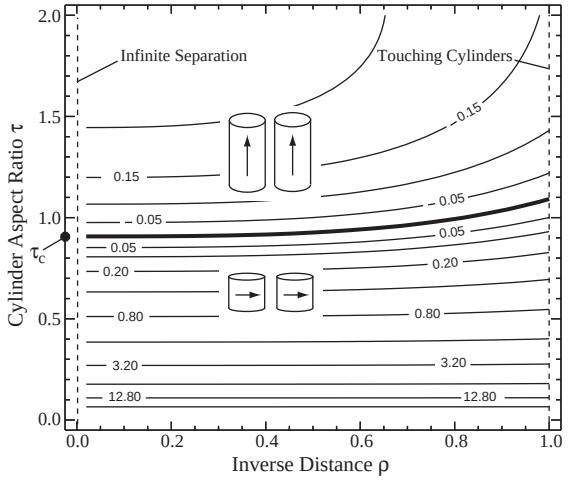

Fig. 7. Contour plot of the difference between the total energies for the vertical and horizontal magnetization states for two interacting cylinders (cases 1 and 2 of Fig. 2) as a function of their inverse distance ρ and aspect ratio τ. The critical aspect ratio $\tau_c(0) = 0.90647$ (infinite separation) slowly increases to $\tau_c(1) = 1.0921$ (cylinders in contact).

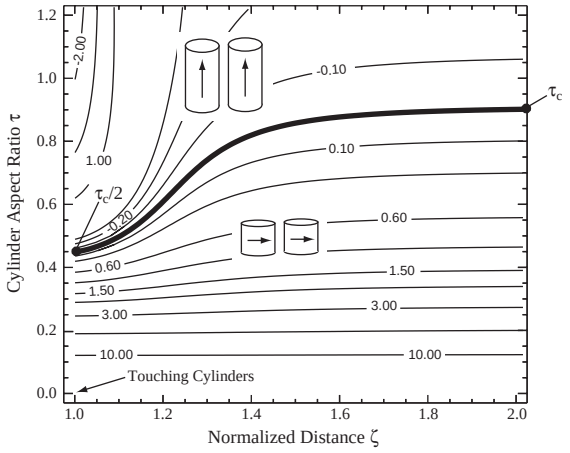

Fig. 8. Contour plot of the difference between the total energies for the vertical and horizontal magnetization states for two interacting cylinders (cases 3 and 4 of Fig. 2) as a function of their distance ζ and aspect ratio τ. The critical aspect ratio $\tau_c(\infty) = 0.90647$ (infinite separation) slowly decreases to $\tau_c(1) = \tau_c(\infty)/2 = 0.45323$ (cylinders in contact).

For cases 3 and 4, Fig. 8 shows a contour plot of $\bar{E}_v^{\mathrm{tot}}(\zeta,\tau) - \bar{E}_h^{\mathrm{tot}}(\zeta,\tau)$, using Eqs. (65) and (67); the thicker contour once again indicates the critical aspect ratio $\tau_c(\zeta)$. When the cylinders

touch, the critical aspect ratio $\tau_c(1) = \tau_c/2 = 0.45323$, which indicates that the axial magnetization state is stabilized with respect to the in-plane configuration.

6. Nanowires

Magnetic nanowires, namely elongated cylinders with a very large aspect ratio, are described in this section. While the most general energy expression of cylinders with axial magnetization was derived in a previous section, often real nanowires resemble more a semi-infinite cylinder rather than a finite one. From an energy point of view, we cannot easily treat nanowires by some limit procedure of the equations already derived, as we have always assumed that two exit poles exist. The sources of the magnetic energy are, in fact, the two poles of the cylinder, or the regions of space where the fringing field is generated. A semi-infinite magnetic nanowire can be described as having a single exit pole, and this difference must show in the energy balance of a single wire or an array of wires.

To show how the two cases, finite and semi-infinite, are different, we consider a cylinder with infinite thickness. This is equivalent to an infinite solenoid, where no fringing field is present (the field is confined within the cylinder surface). Therefore, if we calculate the self-energy of such a structure, we should expect zero. Indeed, starting from the shape amplitude of an infinite cylinder, $D(\mathbf{k}) = 4\pi^2 J_1(k_\perp R)\delta(k_z)$, we can easily verify that the self-energy is zero. On the other hand, taking the limit for $t \to \infty$ after calculating the self-energy for a finite thickness we obtain

$$E_m^{self} = \frac{4}{3}\mu_0 M_0^2 R^3, \tag{68}$$

which is evidently not zero.

Depending on how we approach the calculation of the energy, taking the appropriate limit before or after the integration in Fourier space, we end up with physically different situations. In the case of the finite vs. infinite cylinder, the difference consists in assuming the exit poles at a finite distance, which then goes to infinity (the energy is kept) or assuming that they are at infinity since the beginning and do not generate fringing fields or interact with each other (the energy is lost).

The intermediate case, namely a semi-infinite cylinder, will now be examined in detail. It will be shown that the self-energy is exactly halved with respect to a finite cylinder of very large thickness, and the interaction energy has a monopolar, rather than dipolar, character.

The shape amplitude for a semi-infinite cylinder can be written as

$$D(\mathbf{k}) = \frac{2\pi R}{k} J_1(kR)\left(\pi\delta(k_z) - \mathscr{PV}\left[\frac{1}{ik_z}\right]\right), \tag{69}$$

where the bracketed term is the generalized Fourier transform of a step function (see Ref. [12]) and $\mathscr{PV}$ is the principal value distribution. Plugging the shape amplitude in the expression for the self-energy, and considering the properties of the Dirac-delta distribution, we simply obtain

$$E_m^{self} = \frac{2}{3}\mu_0 M_0^2 R^3, \tag{70}$$

which is the same expression we obtained for a finite cylinder with infinite thickness, just divided by 2. This clearly shows that the sources of the magnetic energy are the poles: now we have neglected one of them (the one positioned at infinity *before* the energy is computed), and the energy is halved.

The same calculation can be performed for the interaction energy, confirming that for two infinite cylinders there is no interaction, for two semi-infinite cylinders we obtain some E^{int}, and for two finite cylinder in the $t \to \infty$ limit, we have $2E^{int}$. The interaction energy can be expressed either from Eq. (58) or by direct computation from Eq. (69), and the final result turns out to be

$$\begin{aligned} E^{int}(r, R) &= \frac{\mu_0}{4\pi}\frac{\Phi_1\Phi_2}{r}\,{}_3F_2\left(\frac{1}{2},\frac{3}{2},\frac{3}{2};2,3;\rho^2\right) \\ &= \frac{\mu_0}{4\pi}\frac{\Phi_1\Phi_2}{r}G_1(\rho), \end{aligned} \tag{71}$$

where we have defined the two "magnetic charges" $\Phi_i = \alpha_i \pi M_i R^2$, which are nothing but the magnetization flux, with correct sign, across the cylinder pole (its flat surface). The function $G_1(\rho)$ is shown in Fig. 3. The interaction energy has a monopolar character, as the $1/r$ term is reminiscent of a

Coulomb interaction, with the usual hypergeometric correction which takes into account the shape anisotropy. In the limit for $R \to 0$, i.e., considering the cylinder as a line of dipoles, we would have obtained a pure Coulomb interaction, as the hypergeometric function goes to 1 in this limit.

It is worthwile to examine the transition between dipolar and monopolar regime in two interacting cylinders. For this purpose, we may calculate the interaction energy in three different ways: (i) as if the two cylinders were dipoles; (ii) by means of Eq. (71); (iii) by the correct full expression equation (58). We choose to evaluate the energy as a function of aspect ratio, and at a fixed distance between the two cylinders $\rho = 4R$. The result is shown in Fig. 9, where the straight dotted line represents E_{mon}, the value of the monopolar approximation (it is obviously a constant, as the monopolar expression is derived in the $\tau \to \infty$ limit and therefore does not depend on τ), the dashed line represents the pure dipole–dipole energy E_{dip} without shape corrections and the solid line is the correct full expression of the interaction energy E which takes into account shape anisotropy. It is evident that when the aspect ratio is small (disks) the dipolar approximation agrees reasonably well with the correct energy, but it soon diverges to arbitrarily large errors when the aspect ratio increases. The residual difference between E and E_{dip}, barely visible near the plot origin, is due to the fact that, for a distance $r = 4R$, the two cylinders cannot be considered as pure dipoles, even for negligible thickness. On the other hand, the energy E appears to converge to the monopolar regime E_{mon} for an aspect ratio around $\tau = 50$ (this value is of course dependent on the chosen distance between the rods: if the energy was evaluated at $\rho = 2R$, the transition between the two regimes would have occurred for a smaller aspect ratio).

These results confirm once more the need for particular care when dealing with magnetostatic coupling between particles when shape anisotropy is present. The deviations from either dipole–dipole or Coulomb interactions are very strong, and if not properly accounted for, the energy evaluation can be affected by an error as high as several orders of magnitude. For example, for two nanowires with aspect ratio of 50 separated by a distance $r = 4R$,

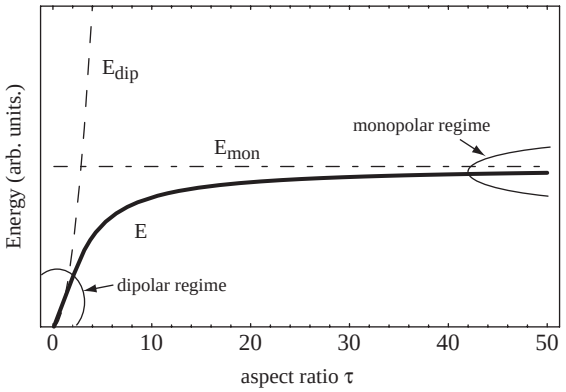

Fig. 9. Comparison between the dipolar and monopolar interaction energies as a function of the cylinder aspect ratio τ, for a cylinder separation distance of $4R$. The thick solid line labeled E represents the exact interaction energy, while E_{dip} and E_{mon} represent the dipolar and monopolar approximations, respectively.

the ratio E_{dip}/E is 320, while the monopolar energy agrees reasonably well ($E_{\mathrm{mon}}/E = 1.04$). For an intermediate case (not easily approximable in either way) of $\tau = 10$, the ratio E_{dip}/E is roughly 15, while the ratio E_{mon}/E is 1.24.

7. Conclusions

It has been shown how a Fourier space approach can describe the magnetostatic coupling between magnetic nanoparticles of arbitrary shape and magnetization state. The main advantages of this approach, compared to the standard real-space evaluation of a double volume integral, are (i) an easy and compact mathematical treatment of shape anisotropy, (ii) the accuracy of the results is related to the number of pixels in the 3D computational arrays rather than to numerical precision in the evaluation of the integrals, and (iii) the availability of advanced FFT algorithms, which can efficiently evaluate the various real-space quantities.

The main conclusion to be drawn from the results presented in this paper is, except for the general expressions of self- and interaction energies, the modified expression (38) for the interaction energy between two particles of identical rotationally symmetric shape. Because of the

cylindrical symmetry, the angular dependence can be separated from the other coordinates, resulting in a dipole–dipole-like expression. While the correction factors $S_i(r,z;\mathbf{s})$ can be determined analytically for a circular disk, as shown in Section 5, numerical evaluation of these integrals (Eqs. (39)–(42)) should be possible for a wide range of particle shapes, including prolate and oblate rotational ellipsoids, tori with either rectangular or circular cross-sections, and truncated cones and paraboloids. The expressions can also be generalized to the case where the two objects do not have the same orientation in space. This would significantly complicate analytical evaluation of the integrals, but should have no effect on numerical evaluations.

Finally, a Fourier space representation of the magnetization immediately suggests the inclusion of time-dependent phenomena, i.e., spin waves. In fact, the approach presented in this paper can be considered as a static spin wave analysis of the particle magnetization distribution. Work is now in progress to extend the framework to spin wave dynamics, generalizing the approach first introduced by Suhl [13].

Acknowledgements

The authors would like to acknowledge the US Department of Energy, Basic Energy Sciences, for financial support under Contract Nos. DE-FG02-01ER45893 and DE-AC02-98CH10886.

Appendix

In this appendix, we prove that the functions $S_1(r,z;R,t)$ and $S_2(r,z;R,t)$ are identical in the limit $r\to 0$, i.e.,

$$\lim_{r\to 0} S_1(r,z;R,t) = \lim_{r\to 0} S_2(r,z;R,t).$$

Working out the k_z integrals for Eqs. (39) and (40), and using Eq. (45), we find

$$S_1(r,z;R,t) = \frac{4\pi^2\rho^3 R}{rV^2}\int_0^\infty \mathrm{d}k\,\frac{J_1(kr)J_1(kR)}{k^2} \times \left[\mathrm{e}^{(d-z)k} - \mathrm{e}^{-(d+z)k}\right],$$

$$S_2(r,z;R,t) = \frac{4\pi^2\rho^5 R}{(r^2-2z^2)V^2}\int_0^\infty \mathrm{d}k\,\frac{J_0(kr)J_1(kR)}{k} \times \left[\mathrm{e}^{-(d+z)k} - \mathrm{e}^{(d-z)k}\right].$$

Taking the difference between the two integrals and ignoring constant pre-factors we find

$$S_1 - S_2 \approx \int_0^\infty \frac{\mathrm{d}k}{k}\left[\frac{r^2+z^2}{r^2-2z^2}J_0(kr) + \frac{J_1(kr)}{kr}\right]J_1(kR) \times \left[\mathrm{e}^{-(d+z)k} - \mathrm{e}^{(d-z)k}\right].$$

Taking the limit for $r\to 0$, the factor between square brackets becomes

$$\lim_{r\to 0}\left[\frac{r^2+z^2}{r^2-2z^2}J_0(kr) + \frac{J_1(kr)}{kr}\right] = \lim_{r\to 0}\left[-\frac{1}{2}J_0(kr) + \frac{J_1(kr)}{kr}\right]$$

and since $\lim_{r\to 0} J_0(kr) = 1$ and $\lim_{r\to 0} J_1(kr)/kr = \frac{1}{2}$ we find that, for the cylinder, $S_1 = S_2$ when $r = 0$.

References

[1] J.L. Simonds, Phys. Today 48 (4) (1995) 26.
[2] H.S. Nalwa (Ed.), Magnetic Nanostructures, American Scientific Publishers, Los Angeles, 2002.
[3] A. Sugurawa, M.R. Sheinfein, Phys. Rev. B 66 (1997) R4899.
[4] A. Aharoni, Introduction to the Theory of Ferromagnetism, 2nd Edition, Oxford University Press, Oxford, 2000.
[5] M. Beleggia, M. De Graef, J. Magn. Magn. Mater. 263 (2003) L1.
[6] S. Tandon, M. Beleggia, Y. Zhu, M. De Graef, J. Magn. Magn. Mater. 271 (2004) 21.
[7] S. Tandon, M. Beleggia, Y. Zhu, M. De Graef, J. Magn. Magn. Mater. 271 (2004) 9.
[8] A. Fert, L. Piraux, J. Magn. Magn. Mater. 200 (1999) 338.
[9] T.G. Sorop, C. Untiedt, F. Luis, M. Kröll, M. Rasa, L.J. de Jongh, Phys. Rev. B 67 (2003) 014402.
[10] M. Beleggia, Y. Zhu, Philos. Mag. B 83 (2003) 1143.
[11] A.J. Bennet, J.M. Xu, Appl. Phys. Lett. 82 (2003) 2503.
[12] W.A. Woyczynski, A.I. Saichev, Distributions in the Physical and Engineering Sciences, Birkhauser, Basel, 1997.
[13] H. Suhl, J. Phys. Chem. Solids 1 (1956) 209.